HHS Public Access

Author manuscript

Mol Neurobiol. Author manuscript; available in PMC 2021 May 01.

Published in final edited form as:

Mol Neurobiol. 2020 May ; 57(5): 2447–2460. doi:10.1007/s12035-020-01894-6.

Genetic ablation of hematopoietic cell kinase accelerates Alzheimer's disease-like neuropathology in Tg2576 mice

Siok Lam Lim[1,2], **Diana Nguyen Tran**[2], **Zanett Kieu**[2], **Christine Chen**[2], **Emmanuel Villanueva**[2], **Sagar Ghiaar**[2], **Victoria Gallup**[2], **Joannee Zumkehr**[1,2], **David H. Cribbs**[3], **Carlos J. Rodriguez-Ortiz**[1,2], **Masashi Kitazawa**[1,2,*]

[1]Center for Occupational and Environmental Health, Department of Medicine, University of California, Irvine, CA 92617, USA

[2]Molecular and Cell Biology, University of California, Merced, CA 95340, USA

[3]Department of Neurology, University of California, Irvine, CA 92697, USA

Abstract

Microglial dysregulation, pertaining to impairment in phagocytosis, clearance and containment of amyloid-β (Aβ), and activation of neuroinflammation, have been posited to contribute to the pathogenesis of Alzheimer's disease (AD). Detailed cellular mechanisms that are disrupted during the disease course to display such impairment in microglia, however, remain largely undetermined. We hypothesize that loss of hematopoietic cell kinase (HCK), a phagocytosis-regulating member of the Src family tyrosine kinases that mediate signals from triggering receptor expressed on myeloid cells 2 and other immunoreceptors, impairs microglial homeostasis and Aβ clearance, leading to the accelerated buildup of Aβ pathology and cognitive decline during the early stage of neuropathological development. To elucidate the pivotal role of HCK in AD, we generated a constitutive knockout of HCK in Tg2576 mouse model of AD. We found that HCK deficiency accelerated cognitive decline along with elevated Aβ level and plaque burden, attenuated microglial Aβ phagocytosis, induced iNOS expression in microglial clusters, and reduced pre-synaptic protein at the hippocampal regions. Our findings substantiate that HCK plays a prominent role in regulating microglial neuroprotective functions and attenuating early AD neuropathology.

Keywords

Microglia; Alzheimer's disease; Hematopoietic cell kinase; Amyloid-β; Tg2576 mice

[*]**Corresponding author:** Masashi Kitazawa, Ph.D., Associate Professor, Center for Occupational and Environmental Health, Department of Medicine, University of California, Irvine, 100 Theory Dr., Suite 100, Irvine, CA 92617, 949-824-1255, kitazawa@uci.edu.

Authorships

All protein extraction, MSD, western blot analysis, and statistical analyses were conducted by SLL. Guidance on microdissection, and immunostaining were provided by JZ. Animal husbandry and genotyping were done by SLL, ZK, EV and CC, and tissue collection were conducted by SLL, ZK, JZ and CJRO. Behavioral tests were designed by CJRO and executed by CJRO and SLL. NOR and OIP scoring were done by SLL and CC. Tissue sectioning was done by ZK, CC and SG, while immunostaining, imaging and analyses were done by SLL, DNT, CC and VG. Experiments were conceived and designed by MK and SLL. Manuscript was written by SLL and critically reviewed by MK. All authors read and approved the final manuscript.

Conflict of interest statement

exThe authors declare that they have no competing interests.

Introduction

Alzheimer's disease (AD) is the most common neurodegenerative disorder plaguing on the aging population worldwide with accelerating prevalence [1]. Although the exact disease-causing mechanisms remain to be determined, emerging evidence from recent human genetics and animal studies have posited that microglia, the primary brain-residing innate immune cells, play a pivotal disease-modifying role in the pathogenesis of AD [2–6]. During the early stage of AD, microglia have been involved in the effective containment and clearance of toxic amyloid-beta (Aβ) species, eliciting neuroprotective functions against the disease [2, 7, 8]. However, as the disease progresses, a subset of microglia displays neurodegenerative phenotypes, presumably through chronic activation by Aβ species, that promotes neuroinflammation [9, 10], further buildup of Aβ [7, 11, 12], propagation of tau [13], synapse loss [14, 15] and cognitive decline [15, 16].

These differential roles of microglia during the disease course may be explained in part by the altered activation of their surface receptors, such as triggering receptor expressed on myeloid cells 2 (TREM2), and the downstream cascades of protein kinases within microglia [17, 18]. Hematopoietic cell kinase (HCK) is a member of the Src family tyrosine kinases (SFKs) and one of the key regulators of phagocytosis among the SFKs in myeloid cells [19, 20]. In the brain, HCK is preferentially expressed in microglia [21, 22] and mediates immunoreceptor (IR)-induced signaling pathways [23, 24], including Aβ-stimulated microglial phagocytosis [7]. Lately, HCK has been implicated in AD based on genetic studies on late-onset AD patients [21] and $APP^{NL\text{-}G\text{-}F/NL\text{-}G\text{-}F}$ transgenic mouse model of AD [25]. In addition, TREM2, Fc fragment of IgE receptor Ig (FCER1G), and spleen tyrosine kinase (SYK), which are found up- and downstream of HCK signaling, have been identified as AD-associated human microglial genes, thereby underscoring the involvement of microglial HCK signaling pathway in AD pathogenesis [26].

Using *in vitro* and *in vivo* approaches, we recently demonstrated that the inhibition of HCK signaling in microglia impaired phagocytic clearance and containment of Aβ, hence accelerated buildup of Aβ plaques in the brain while cognition was spared in J20 mouse model of AD [7]. Given that the development of plaque pathology and associated inflammatory activation around plaques could be highly variable among young J20 mice, especially at the initial growth stage of plaques, we sought to validate the neuroprotective role of HCK in another mouse model of AD. In this study, we used Tg2576 mice, a widely used and well characterized mouse model, whose Aβ plaque pathology develops at 9–12 months of age [27]. We hypothesize that ablation of HCK impairs microglial phagocytosis and Aβ clearance, leading to accelerated development of AD neuropathology and cognitive decline. The current study allows us to rigorously test our hypothesis, validate reproducibility of our earlier study, as well as stratified the genetic findings of others which implicate microglial HCK as AD-related gene [21, 25, 26]. Our findings will provide invaluable insights for incorporating HCK signaling pathway as a therapeutic avenue for treating AD.

Materials and methods

Animals

HCK knockout (HCK-KO) mice were generously provided by Dr. Clifford Lowell (University of California, San Francisco), while hemizygous hamster prion protein-$hAPP_{K670N/M671L}$ Tg2576 mice were kindly provided by Dr. David H. Cribbs (University of California, Irvine). Wild-type (WT) mice were purchased from Jackson Laboratory. HCK-deficient Tg2576 (Tg/HCK-KO) mice was generated by crossing Tg2576 mice with HCK-KO mice, and the colony was expanded by crossing Tg/HCK-KO mice with HCK-KO mice. WT and HCK-KO mice were of C57BL/6 background, whilst Tg2576 and Tg/HCK-KO mice were of C57B6/SJL background. To check for possible changes in the genetic background during crossbreeding, we used littermates of HCK-KO and Tg/HCK-KO mice for the study. Mice were inbred for less than 4 generations to prevent genetic drift. Both genders were used in this study, but the number of each gender used does not provide sufficient statistical power to test for gender effects. Mice were analyzed at 10–13 months old when they are at an early stage of pathological development. All animal studies performed were approved by the University of California Institutional Animal Care and Use Committee and were in accordance with Federal guidelines.

Novel Object Recognition (NOR)

NOR was conducted as previously described [7, 28] with some modifications. Mice were first habituated to the trainer by handling them for 2 mins each in three consecutive days. The mice handling was then extended to another 5 mins of habituation to a Plexiglas arena without objects. After five consecutive days of habituation (day nine of the training), mice were habituated to the training room for 15 mins before task training and 2 h after (for memory retention). Mice were trained by exposing them to two identical objects placed side-by-side in the arena for 10 mins. At 24 h later, mice were allowed to explore one familiar object (ie. object exposed before) and one novel (new) object in the arena for 5 mins. Mice activities in the arena were recorded using video camera, which was later replayed to determine their exploration behaviors and quantified as recognition index. Recognition index (RI) indicates the relative time mouse spent in exploring the novel object, and significance from RI of 0.5 (chance level) using one sample *t* test denotes novel object recognition. Exploration was considered when mouse pointed its head towards an object at a distance of < 2.5 cm with its neck extended and vibrissae moving. Simple proximity, chewing and sitting on objects were not considered as exploratory behaviors. Mice that did not explore both objects during training were not used for behavioral analysis. Objects used in this task were carefully selected to prevent preference or phobic behaviors. To eliminate olfactory cues, the objects and arena were thoroughly cleaned with 70% ethanol and the beddings were removed of droppings and stirred between mice.

Object In Place (OIP)

OIP training was conducted on the day after NOR test, with similar procedures except for the set of objects used and the object placement. During task training, a new set of identical objects were placed side-by-side in the arena for mice to explore for 10 mins. 24 h later, mice were exposed to the same set of identical objects, with one of the objects moved to

either the left or right side of the arena. RI for OIP indicates the relative time mouse spent in exploring the object at the novel place.

Morris Water Maze (MWM)

MWM was conducted as described previously [7, 28] with some modifications. Mice were trained to locate a circular and transparent Plexiglas platform submerged at 1 cm beneath the surface of the water, which was invisible to them when they were swimming in the 1 m diameter water tank. The platform was placed in an equidistant position in a quadrant of the circular tank, and visual cues were placed on three sides of the wall for spatial reference. Mice were subjected to six training trials per day for five consecutive days whereby WT mice of 10–12 months old reached the training criterion of 25 s in escape latency by the fifth day of training. On the first two days of training, mice were placed on the platform for 30 s, and allowed to rest for 30 s in a dry cage. Trials involved placing the mice into the tank at one of the four designated starting points in a pseudorandom order. Mice were given up to 60 s to swim to the platform. If they failed to do so, they were be manually guided to the platform. Once on the platform, they were left there for another 30 s, before being transferred to a dry cage to rest for 30 s. On Day three of the training, mice were placed directly into the tank without prior placement on the platform. At 72 h after the last training, the platform was removed and mice were tested by placing in the tank at the quadrant opposite of where the platform was supposed to be. At 60 s, mice were removed from the tank and allowed to rest for 30 s. Mice were next returned to the tank at the same location, but with the platform in the place this round. At one week after the last training, mice were again tested with platform removed from the tank. All MWM trainings and tests were recorded by video camera and analyzed using VideoTrack system (ViewPoint Behavior Technology). Behavioral performance was quantified in terms of escape latency (time taken to reach area occupied by platform during training), number of platform crosses (number of times mouse crosses the platform area during the 60 s), and % time spent in the target (with platform) and opposite (from platform) quadrants.

Tissue collection

Littermates of Tg2576 and WT mice, as well as HCK-KO and Tg/HCK-KO mice were euthanized at 11–13 months old after behavioral studies at 10–12 months of age. Mice were perfused with ice-cold PBS and the brains were collected in one of the two ways as followed: i) for immunostaining, the hemibrain was fixed with 4% PFA; iii) for biochemical analyses, the hemibrain was microdissected into hippocampus and cortex, and frozen at −80°C until further processing.

Immunohistochemical analysis

Hemibrains designated for immunostaining were cryopreserved in −80°C after fixing in 4% PFA and cryoprotected in 30% sucrose for 2–3 days each. Thereafter, hemibrains were sectioned coronally at 20 μm using a freezing microtome (SM2010R; Leica Biosystems) and sections were stored in PBS with 0.05% sodium azide at 4°C. Sections from different mice at bregma position −2.54 mm (according to the mouse brain atlas of Franklin and Paxinos, Third Edition, 2007) were then mounted on microscopic slides and processed under the

same conditions. Negative control slides were prepared by omitting primary antibodies to check for non-specific labeling.

To label synaptic proteins, synaptophysin (Abcam, catalog # ab14692, 1:750 dilution) and PSD95 (NeuroMab, catalog # 75028, 1:750 dilution) antibodies were applied to three sections (from bregma −2.54 mm and at 10 sections anterior or posterior to that) per mouse, followed by Alexa Fluor 555 and 633 conjugated secondary antibodies (Life Technologies Corporation, catalog # A21429 and A21052, 1:200 dilution), respectively. Using a 20x objective on the EVOS FL Cell Imaging System as previously described [7, 29], fluorescence signals from the proteins in three different areas in the DG, and two of each in the CA1 and CA3 regions were imaged, after setting the intensity cutoff on the microscope using negative control sections. Fluorescence detected after eliminating the background signal yields positive signal from the synaptic protein. In each image, five 50 × 50 pixel area were selected from the four corners and the middle of the image that best represent the protein intensity of the region and were quantified using ImageJ. An average of all areas from each region was calculated and represented the synaptic protein intensities in the DG, CA1 and CA3 regions of the hippocampus. Data are expressed as % synaptic protein intensities per genotype relative to that of HCK-KO mice as the tissues were sectioned in two batches that they labeled with the antibodies differently. Both batches of tissues consisted of HCK-KO mice as a normalizing control.

To assess for Aβ plaque burden, four additional sections (at every 10 sections anterior or posterior from bregma −2.54 mm) per mouse were pretreated with 90% formic acid for 5 mins as previously described [7, 30], before incubated in 4G8 (Covance Inc., catalog # SIG-39220, 1:1000 dilution) Aβ plaque antibody. Aβ plaques were then visualized using either colorimetric or immunofluorescence method which allows double or triple-labeling of other proteins on the same section. For colorimetric method, ABC Peroxidase Standard Staining Kit (Thermo Fisher Scientific Inc.) and DAB Peroxidase Substrate Kit (Vector Laboratories) were applied on the sections and labeled plaques were imaged on EVOS XL Core Imaging System (Thermo Fisher Scientific Inc.). For immunofluorescent labeling of primary antibodies, Alexa Fluor 488, 555 or 633 conjugated secondary antibodies (Life Technologies Corporation) raised in corresponding species were applied to the sections. All sections were also stained with DAPI for nuclear labeling. Fluorescent images were taken with either BZ-9000 All-in-one Fluorescence Microscope (KEYENCE Corp. of America) or confocal laser microscope (DM2500; Leica Microsystems) when volumetric analysis was required. For Aβ plaque burden analysis, similar regions between sections in the hippocampus, cortex near CA1 and CA3, entorhinal cortex and amygdala were being imaged. Plaque areas were quantified using ImageJ software, and plaque burden was calculated by taking % of plaque areas over the entire area of the image field. To label Thioflavin-S plaques, sections were stained for 10 min in 0.5% Thioflavin-S (Sigma-Aldrich, catalog # T1892) in 50% ethanol (in the dark) without formic acid treatment. Thioflavin-S plaques were captured with confocal microscope using a 40x objective with 2x zoom in 1 μm z-separation step. Plaque sphericity was quantified using the Imaris software (Bitplane Inc.) to assess the diffusivity of plaques.

To assess for microglial activities around 4G8$^+$ or Thioflavin-S plaques, Iba-1 (FUJIFILM Wako Chemicals USA, Inc., catalog # 019–19741, 1:500 dilution) primary antibody was used, and was quantified at about 20 μm from the edge of the plaque (diameter ≥ 30 μm), which included the area of the plaque itself and any whole microglia within the region [7, 31]. CD68 (Bio-Rad AbD Serotec Limited, catalog # MCA1957, 1:100 dilution) primary antibody was applied to assess the activation of phagolysosomes in microglial cells after Aβ phagocytosis. To determine Aβ internalization ratio, volume of Aβ found within CD68$^+$ phagolysosomes in Iba1$^+$ microglia was normalized to microglial number on the plaque(s) and Aβ plaque volume within the region [7, 32]. pSYK (Tyr525/526; Cell Signaling Technology, catalog # 2710, 1:100 dilution) and iNOS (BD Transduction Laboratories, catalog # 610431, 1:500 dilution) antibodies were also used to assess activation of SYK and pro-inflammatory state of CD11b$^+$ (Bio-Rad AbD Serotec Limited, catalog # MCA74GA, 1:100 dilution) microglia clustering around plaques, respectively. Aβ plaques of diameter ≥ 30 μm or microglial clusters found throughout the hemibrain of the coronal section (excluding the thalamus) were assessed for these studies. Parameters reflecting microglial phenotypes around plaques were quantified and averaged from multiple regions for each mouse, before comparing the mean values between genotypes. Area covered by respective proteins were measured using ImageJ, while volumetric image measurements, microglial number and morphology were made using Imaris software as previously described [7, 32].

Protein extraction and western blot analysis

Protein was extracted from hippocampus by homogenizing in T-PER Tissue Protein Extraction Reagent (Thermo Fisher Scientific Inc.) complemented with protease and phosphatase inhibitors (MilliporeSigma), followed by centrifugation at 100,000*g* for 1 h at 4 °C to get detergent-soluble fraction and –insoluble pellet. Pellet was further homogenized in 70% formic acid and centrifuged as before to collect detergent-insoluble fraction. All protein fractions were stored at −80°C until further analysis.

Protein concentration from hippocampus in detergent-soluble fractions were measured using the Bradford protein assay. Standardized protein mass were separated by SDS-PAGE and transferred to Immobilon-FL PVDF membrane (EMD Millipore). Membranes were blocked in Odyssey Blocking Buffer (LI-COR Biosciences) for 1 h at room temperature, before immunoblotted overnight with shaking at 4°C with the following antibodies diluted in Odyssey Blocking Buffer with 0.2% Tween 20 (Thermo Fisher Scientific Inc.): synaptophysin (Abcam, catalog # ab14692, 1:1000 dilution), PSD95 (NeuroMab, catalog # 75028, 1:1000 dilution), 6E10 (Covance Inc., catalog # SIG-39320, 1:1000 dilution), CT20 (Calbiochem, catalog # 171610, 1:1000 dilution) and beta-site amyloid precursor protein cleaving enzyme 1 (BACE1; Calbiochem, catalog # 195111, 1:2000 dilution), GAPDH (Santa Cruz Biotechnology Inc., catalog # sc-25778, 1:5000 dilution) or tubulin (Sigma-Aldrich, catalog # T6074, 1:25000 dilution). Membranes were then washed in TBST, before incubated with corresponding IRDye secondary antibodies (LI-COR Biosciences) diluted in TBST/SDS and 5% fat-free milk for 1 h at room temperature. Membranes were washed in TBST thereafter and scanned using Odyssey Imaging System (LI-COR Biosciences). Band intensities were quantified with Image Studio software (version 5.2, LI-COR Biosciences) and normalized to that of GAPDH or tubulin which serves as protein loading control.

Quantitative analysis of Aβ by Meso Scale Discovery (MSD)

Aβ38, Aβ40 and Aβ42 were quantified in both detergent-soluble and –insoluble fractions using the V-PLEX Plus Aβ Peptide Panel 1 (4G8) Kit (Meso Scale Discovery). Aβ38, Aβ40 and Aβ42 peptide calibrators, three neurodegeneration controls, and protein fractions were loaded onto the MSD MULTI-SPOT® 96-Well 4-Spot plate, after the addition of detection antibody solution. Detergent-soluble fractions were loaded directly onto the 96-Well 4-Spot plate, while detergent-insoluble fractions were diluted 1:40 in neutralization buffer (1 M Tris-base and 0.5 M Na_2HPO_4) before loading. Plate was read on a SECTOR® Imager plate reader (MSD) after 2 h incubation, washed, and loaded with Read Buffer T. Respective species of Aβ concentration were calculated with reference to their standard curves, and expressed as femtogram per microgram of protein for detergent-soluble fractions or picogram per milligram of tissue for detergent-insoluble fractions.

Statistical analysis

All data are presented as mean ± SEM, and statistical analyses were done using GraphPad Prism 6. Values that were not within the predetermined criterion of two SDs from the mean were considered statistical outliers and were excluded from the analysis. Unpaired *t* test with Welch's correction (two-tailed) was used for comparison of means of two groups. For comparisons between three or more groups, one-way ANOVA or two-way ANOVA (for two factors) with Fisher's LSD *post hoc* test was used to evaluate statistical significance, unless otherwise stated. Data with $p < 0.05$ was considered statistically significant. To determine the number of mice needed to reach statistical difference, power analysis was conducted, and sufficient number of mice was used in this study.

Results

Genetic ablation of HCK in Tg2576 mice impaired their performance in MWM task

We have recently investigated the role of HCK in young J20 mouse model of AD [7]. To rigorously test our hypothesis and confirm reproducibility of our earlier findings, we examined the role of HCK in another widely used mouse model of Aβ pathology - Tg2576 mice. First, we determined whether HCK deficiency accelerated cognitive decline in Tg2576 mice. When we tested mice for non-spatial recognition memory (NOR) and spatial recognition memory (OIP and MWM), no significant differences were detected in WT, HCK-KO, Tg2576, and Tg/HCK-KO mice in NOR or OIP tests (Fig. S1a, b). In MWM, on the other hand, Tg/HCK-KO mice consistently exhibited significantly impaired acquisition memory, starting from Day two of the training to Day five, as compared to WT mice (Day two: $p = 0.0037$, Day three: $p = 0.0078$, Day five: $p = 0.0009$), HCK-KO mice (Day two: $p = 0.0152$, Day three: $p = 0.0031$, Day four: $p = 0.0026$, Day five: $p = 0.0008$), or Tg2576 mice (Day two: $p = 0.0009$, Day three: $p = 0.0045$, Day four: $p = 0.0135$, Day five: $p = 0.0113$) mice (Repeated measures two-way ANOVA with multiple comparisons of performance by genotype per day; Fig. 1a). At 1 wk, but not 72 h (data not shown) after the last training in MWM, Tg/HCK-KO mice again took drastically longer escape latency than the other three genotypes in locating the hidden platform (WT mice: $p = 0.0359$, HCK-KO mice: $p = 0.0083$, Tg/HCK-KO mice: $p = 0.0149$, Fisher's LSD *post hoc* test; Fig. 1b). Interestingly, in terms of the number of platform crosses, Tg/HCK-KO mice crossed substantially fewer

times than HCK-KO mice only ($p = 0.0031$, Fisher's LSD *post hoc* test) at 72 h (data not shown), but crossed almost significantly fewer times than Tg2576 mice at 1 wk post-training ($p = 0.0541$, one-way ANOVA, $p = 0.0064$, Fisher's LSD *post hoc* test; Fig. 1c). In accordance, Tg/HCK-KO mice spent the least % time in the target quadrant than the other three genotypes at the two time-points, however, it was not statistically significant ($p = 0.2032$ for 72 h, $p = 0.3309$ for 1 wk, one-way ANOVA; Fig. 1d for 1 wk test). In terms of % time spent in opposite quadrant, Tg/HCK-KO mice spent the most time in that quadrant than the other three genotypes at both time points, but it was only significant against WT ($p = 0.0178$, Fisher's LSD *post hoc* test) and HCK-KO ($p = 0.001$, Fisher's LSD *post hoc* test) mice at 1 wk post-training (Fig. 1e). All mouse genotypes completed the 1 wk MWM test with no apparent differences in the total distance moved (Fig. S1c) or in the swim speed (Fig. S1d). Taken together, our 1 wk MWM test revealed that HCK deficiency in Tg2576 mice significantly impaired their long-term spatial memory.

HCK deficiency in Tg2576 mice reduced hippocampal pre-synaptic protein

Given that one of the pathological features of AD is synaptic loss which correlates with the severity of cognitive deficits in AD patients [33, 34], we investigated whether genetic deletion of HCK in Tg2576 mice would alter the spatial expression of pre-synaptic (synaptophysin) and post-synaptic (PSD95) proteins. Synaptophysin immunoreactivity was significantly reduced in the hippocampal CA1 ($p = 0.0025$ vs WT mice, Fisher's LSD *post hoc* test) and CA3 ($p = 0.0048$ vs WT mice, $p = 0.0343$ vs Tg2576 mice, Fisher's LSD *post hoc* test) regions, as well as in all three regions ($p = 0.0032$ vs WT mice, $p = 0.0458$ vs Tg2576 mice, Fisher's LSD *post hoc* test), including that of DG which showed the least % intensity among the genotypes (Fig. 2a, b). Similarly, PSD95 immunoreactivity in Tg/HCK-KO mice showed the least, though not significant, % intensity in the DG ($p = 0.6312$, one-way ANOVA), CA1 ($p = 0.3922$, one-way ANOVA) and CA3 ($p = 0.4927$, one-way ANOVA) regions among all genotypes (Fig. S2a, b). There were, however, no apparent differences in the overall protein levels of synaptophysin and PSD95 between the mouse genotypes (Fig. S2c, d). There is a possibility that subtle changes in the protein expression was detected spatially via immunofluorescence, but not from the whole hemibrain lysate as measured by western blot analysis.

Eliminating HCK in Tg2576 mice significantly augmented Aβ species and plaque burden

We next examined whether the genetic ablation of HCK exacerbated AD-like neuropathology at early plaque stage in the mouse model. Areas of Aβ plaques were measured in the hippocampus, cortex, entorhinal cortex or amygdala region of the hemibrain, and taken relative to the entire area of the image as Aβ plaque burden. There were a two- ($p = 0.0909$) and three-fold ($p = 0.0689$) increase in 4G8-positive plaque burden in the cortex and entorhinal cortex regions, respectively, of 11–13 months old Tg/HCK-KO mice when compared to age-matched Tg2576 mice (Fig. 3a, b). However, the increment only became significant ($p = 0.0201$) when the means of all assessed regions were taken (Fig. 3b).

Given that the hippocampus is one of the earliest brain regions to be affected in AD [35] as well as in Tg2576 mice [27, 36], we quantified the level of Aβ38, Aβ40 and Aβ42 species in

detergent-soluble and -insoluble fractions of mouse hippocampal lysates using Meso Scale Discovery (MSD) analysis. Comparing to Tg2576 mice, Tg/HCK-KO mice exhibited a nearly two-fold increase in either Aβ38 ($p = 0.0234$) or Aβ40 ($p = 0.0246$) levels in the soluble fractions, or in Aβ38 ($p = 0.0058$), Aβ40 ($p = 0.0147$) or Aβ42 ($p = 0.029$) levels in the insoluble fractions (Fig. 3c). However, HCK elimination in from Tg2576 mice did not alter soluble Aβ42 levels significantly ($p = 0.3406$, Fig. 3c) from that of Tg2576 mice. As expected, soluble and insoluble Aβ38, Aβ40 and Aβ42 levels in Tg/HCK-KO mice were significantly higher than that of the WT or HCK-KO mice ($p = 0.0006$ - $p < 0.0001$).

To examine whether the augmented Aβ species were mediated by increase generation of Aβ in Tg/HCK-KO mice, we quantified full length amyloid precursor protein (APP) and its C-terminal fragments (CTFs: C83 and C99) in the hippocampal lysates. As anticipated, both full length and CTFs APP were highly expressed in Tg2576 and Tg/HCK-KO mice relative to the non-AD mice (Fig. S3a, b). However, there were no apparent differences in the levels observed between Tg2576 and Tg/HCK-KO mice, implicating that HCK deficiency in Tg2576 mice did not modulate APP production nor processing. In corroboration, we found similar level of mature BACE1, a prerequisite enzyme for C99 fragment and Aβ formation [37], in Tg/HCK-KO mice relative to Tg2576 mice ($p = 0.952$, Fig. S3c, d). Taken together, our results suggest that the exacerbated Aβ plaque deposition or Aβ species accumulation in Tg/HCK-KO mice was not likely induced by increased APP production nor enhanced amyloidogenic pathway.

Knocking out HCK in Tg2576 modulated morphological phenotypes and activities in Aβ plaque-associated microglia

Since clusters of activated microglia are commonly observed around Aβ plaques in postmortem human AD brains [11, 38, 39] and in AD mouse models, including Tg2576 mice [40, 41], we examined whether HCK deficiency perturbed such microglial phenotypes. We have previously observed drastic reduction in microglial phagocytosis after pharmacological inhibition of SFKs/HCK in BV2 cells or genetic ablation of HCK in J20 mice [7]. Using confocal microscopy and Imaris volumetric and colocalization analysis, we quantified the volume of 4G8-positive plaques internalized in $Iba1^{+}/CD68^{+}$ microglial phagolysosomes as previously described [7, 32]. Quantitative analysis of the Aβ internalization ratio revealed a significant 74% reduction in microglial phagocytic activity in Tg/HCK-KO mice when compared to Tg2576 mice ($p = 0.0422$, Fig. 4a, b). We also found a 43% reduction in % Ibal-positive microglia clustering on 4G8-positive plaques (ie. microglial coverage, after normalized by plaque volume and microglia number) in Tg/HCK-KO mice ($p = 0.0755$, Fig. 4c). Interestingly, similar number of Ibal-positive microglia with similar processes length and branching were found clustering around 4G8-positive plaques in both genotypes (Fig. 4d–f).

Microglia have been recently reported to play neuroprotective role by containing dense core Thioflavin-S plaques with extended processes, thereby making them more compact and less diffuse [42, 43]. We observed a 24% reduction of Thioflavin-S plaque sphericity ($p = 0.3135$, Fig. S4a, b) in Tg/HCK-KO mice, indicating that HCK deficiency has the propensity of resulting in more diffuse and less compact mature Aβ plaques. However, there was no

change in the volume of Thioflavin-S plaques covered by $Iba1^+$ microglia per plaque volume per microglia between Tg2576 and Tg/HCK-KO mice (Fig. S4c) nor the number (Fig. S4d) or % volume (Fig. S4e) of microglia clustering around Thioflavin-S plaques. Further analysis of the microglial morphology, however, revealed a 29% reduction in the total processes length of the microglia per microglia ($p = 0.0895$, Fig. S4f), with no drastic difference in the branching of the microglia ($p = 0.1231$, Fig. S4g) in Tg/HCK-KO mice relative to Tg2576 mice. These data imply that at the early plaque stage of Tg2576 mice, HCK deficiency elicits moderate modulation on the dense core plaques and their surrounding microglia.

Since the phagocytic capacity (activation) of microglia around plaques were attenuated in HCK ablated Tg2576 mice, we sought to investigate if these microglia around plaques exhibited differential activation states in terms of cellular signaling and inflammatory responses. To correlate with the plaque-associated microglia analyzed in Fig. 4, we examined only microglia that formed clusters and determined the expression levels of iNOS and/or pSYK in CD11b-positive microglial clusters and the number of cells expressing these markers (Fig. 5). Quantitative analyses of these markers did not reveal significant modulation in the expression of either iNOS ($p = 0.1026$, Fig. 5b) or pSYK ($p = 0.1683$, Fig. 5c) in CD11b-positive microglia of Tg/HCK-KO mice relative to age-matched Tg2576 mice. However, when assessing the dual expression of iNOS and pSYK in CD11b-positive microglia, we found a significant increase of 55% in Tg/HCK-KO mice as compared to Tg2576 mice ($p = 0.0132$, Fig. 5d). On the other hand, a substantial decrease in the number of CD11b-positive cells was observed in Tg/HCK-KO mice ($p = 0.0018$, Fig. S5), but did not decrease the number of CD11b-positive microglia expressing iNOS ($p = 0.1894$, Fig. 5e), pSYK ($p = 0.0711$, Fig. 5f) or iNOS and pSYK ($p = 0.1721$, Fig. 5g) significantly. These findings implicate that the HCK ablation augmented SYK and microglial pro-inflammatory activation in microglial clusters around plaques.

Discussion

Emerging genome-wide association studies and gene expression network analysis have associated microglial and immune pathways with AD pathogenesis [4, 6, 21, 26, 44]. Impairment in microglial Aβ phagocytosis has been shown to contribute to Aβ deposition and subsequent AD pathology [45, 46]. Deciphering the molecular mechanisms that derail proper microglial phagocytic activity in AD is thus crucial in delineating the pathogenesis of AD. HCK is a phagocyte-specific tyrosine kinase among the SFKs [19, 20], and is highly expressed by microglia in the brain [21, 22] to mediate microglial activation and function, such as Aβ-stimulated microglial phagocytosis [7]. However, recent genetic studies implicate HCK as AD-related genes as it possesses significant regulatory strength with elevated expression in the microglia of late-onset AD patients [21] as well as in the cortices of $APP^{NL\text{-}G\text{-}F/NL\text{-}G\text{-}F}$ mice [25]. Notwithstanding that, several AD-associated human microglial genes located up- and downstream of HCK/SFKs, respectively, have also been identified, underpinning the importance of microglial HCK signaling pathway in AD pathogenesis [26]. Nonetheless, reports on the molecular assessment of HCK signaling in AD pathogenesis are lacking, and how the neuroprotective role of HCK during early AD

pathogenesis progresses to elevated gene expression during the late-stage of the disease is still a puzzle.

It is noteworthy that HCK is not the only microglial kinase with such dichotomous roles. Augmented expression of microglial phospho-tyrosine and phospho-Src, which mediated proper microglial function, have been reported in AD brains [47, 48], and are likely due to Aβ stimulation of microglia as shown in *in vitro* and in vivo studies [48, 49]. Likewise, high levels of pSyk were expressed in hyperactive microglia of human AD brains and AD mouse models [50, 51], and have been reported to contribute to the secretion of pro-inflammatory cytokines upon stimulation by Aβ species [52, 53]. Given that microglia possess neuroprotective role during the early stage of AD [54] and early intervention of dysfunctional microglial Aβ phagocytosis seems critical for effectiveness [55], we sought to evaluate the critical role of HCK in mediating Aβ clearance and containment during the early phase of the disease.

We have demonstrated for the first time in our previous study that HCK plays a multifactorial role in regulating microglial Aβ phagocytosis and plaque envelopment that facilitate Aβ clearance and containment during the early stage of Aβ plaque deposition in J20 mouse model of AD [7]. We showed that pharmacological inhibition of SFKs/HCK in BV2 cells and genetic ablation of their downstream kinase, SYK, in primary microglia significantly attenuate Aβ oligomers-stimulated microglial phagocytosis. Wherein HCK-deficient J20 mice, we observed exacerbated Aβ plaque burden, reduced microglial phagocytosis of Aβ plaques, and induced iNOS expression in plaque-associated microglial clusters. These observations were recapitulated in the current study where HCK-deficient Tg2576 mice was employed and assessed at the initial stage of plaque pathology.

Intriguingly, ablating HCK genetically in Tg2576 mice elicited cognitive deficits as evident from spatial memory test. This was not observed in the J20 mouse model where neuropathological exacerbation by HCK deficiency did not lead to cognitive failure [7]. We postulate that the difference in APP mutations of the two AD mouse models and the age of the mice studied could have contributed to this disparity. In the previous study, HCK was ablated in J20 mice that carry Swedish and Indiana APP mutation [56] and the cognitive function of the mice were assessed at 5–6 months old [7]. In this study, Tg2576 mice with Swedish APP mutation [27] was ablated of HCK and studied at 10–12 months old. As such, the younger J20 mice with different APP transgene might be more tolerant to pathology-induced cognitive deficits when HCK was ablated.

We noted that our Tg2576 mice of 10–12 months old did not show cognitive deficits during MWM training and test trial, which conflicts with the first report by its creator – Hsiao et al. [27]. On the other hand, King and Arendash reported that Tg2576 mice at up to 19 months old exhibited comparable performance in MWM training and trial with non-transgenic mice [57], as observed in our study. It has been suggested that the divergence in MWM performance of Tg2576 mice could be attributed to factors, such as technical differences in MWM tasks between laboratories, different selection criteria of animals for analysis, or possible progressive genetic drift in the Tg2576 line [58]. While our MWM experiments did not explicitly reveal cognitive impairments in our Tg2576 mice, it was clear that genetic

ablation of HCK in these mice accelerated cognition decline when tested under the same experimental conditions. However, our NOR and OIP tests failed to detect any cognitive differences between the genotypes, possibly due to the lower sensitivity of the tests than MWM that might have hindered the actual reflection of the animal performance. Nonetheless, we are confident that the tests were properly executed as we consistently obtained RI values in the range of 0.55 – 0.6 as reported in WT mice of 5 – 13 months old [59, 60] from a large number of our WT control mice.

While HCK deficiency in Tg2576 mice induced spatial memory impairment, we did not observe drastic alteration in the spatial hippocampal PSD95 levels, even though they were expressed at lower levels in Tg/HCK-KO mice than in Tg2576 mice. On the other hand, substantial reduction of pre-synaptic synaptophysin intensity was observed in the CA3 and overall (DG, CA1 and CA3) regions when HCK was removed from Tg2576 mice. Interestingly, modulation on the pre-synaptic protein alone by HCK deficiency was sufficient to elicit cognitive deficit in Tg/HCK-KO mice, as observed in other study [61]. In our previous study, post-synaptic PSD95 protein, not synaptophysin, was modulated in HCK ablated J20 mice, but that did not lead to cognitive impairment [7]. We do not know for sure the cause in the disparities in the levels of spatial synaptic proteins between the two HCK deleted AD mouse models, but based on reports of others studying microglia phenotypes and Aβ pathology in different AD mouse models [62], we deduce the differences in the APP mutations and the age of the mice analyzed as the likely attributing factors.

The current study supports our previous findings that HCK plays a multifactorial neuroprotective role in regulating microglial Aβ phagocytosis and plaque containment that facilitate Aβ clearance and confinement during the early stage of plaque pathology. Ablating HCK in Tg2576 mice resulted in exacerbated Aβ deposition and spatial memory cognitive impairments, despite the presence of other members of the SFKs that could compensate for the function of HCK. Furthermore, significant activation of the pro-inflammatory state microglia was observed, implicating that depleting of HCK alone is sufficient to accelerate microglia class switch from neuroprotective phenotype to neuroinflammation type, which is usually observed in AD mouse model and patients (Fig. 6). With microglia-driven phagocytosis and neuroinflammation as critical mechanisms associated with AD [63], our studies strongly suggest HCK as a therapeutic target for early intervention of the disease.

Supplementary Material

Refer to Web version on PubMed Central for supplementary material.

Acknowledgements

We thank the following people for their kind contribution and assistance: Dr. Clifford Lowell (University of California, San Francisco) for the HCK-KO mice; Dr. David H. Cribbs (University of California, Irvine) for the Tg2576 mice; Dr. David Baglietto-Vargas (University of California, Irvine) for his technical support on Confocal Microscopy, and Dr. Samuel E. Marsh (University of California, Irvine) for his guidance on Imaris analysis.

Funding information

This study was supported by the National Institute of Health/National Institute of Environmental Health Sciences (R01 ES024331) and Alzheimer's Association (NIRG-12-242598 and AARF-16-440554).

References

1. Lane C, Hardy J, Schott J (2018) Alzheimer's disease. Eur J Neurol 25:59–70. 10.1016/j.med.2019.03.012 [PubMed: 28872215]
2. Hansen DV, Hanson JE, Sheng M (2018) Microglia in Alzheimer's disease. J Cell Biol 217:459–472. 10.1083/jcb.201709069 [PubMed: 29196460]
3. Colonna M, Butovsky O (2017) Microglia function in the central nervous system during health and neurodegeneration. Annu Rev Immunol 35:441–468. 10.1146/annurev-immunol-051116-052358 [PubMed: 28226226]
4. Efthymiou AG, Goate AM (2017) Late onset Alzheimer's disease genetics implicates microglial pathways in disease risk. Mol Neurodegener 12:43 10.1186/s13024-017-0184-x [PubMed: 28549481]
5. Sims R, Van Der Lee SJ, Naj AC, et al. (2017) Rare coding variants in PLCG2, ABI3, and TREM2 implicate microglial-mediated innate immunity in Alzheimer's disease. Nat Genet 49:1373–1384. 10.1038/ng.3916 [PubMed: 28714976]
6. Sala Frigerio Carlo, Wolfs L, Fattorelli N, et al. (2019) The Major Risk Factors for Alzheimer's Disease: Age, Sex, and Genes Modulate the Microglia Response to Aβ Plaques. Cell Rep 27:1293–1306. 10.1016/j.celrep.2019.03.099 [PubMed: 31018141]
7. Lim SL, Tran DN, Zumkehr J, et al. (2018) Inhibition of hematopoietic cell kinase dysregulates microglial function and accelerates early stage Alzheimer's disease-like neuropathology. Glia 66:2700–2718. 10.1002/glia.23522 [PubMed: 30277607]
8. Wang Y, Ulland TK, Ulrich JD, et al. (2016) TREM2-mediated early microglial response limits diffusion and toxicity of amyloid plaques. J Exp Med 213:667–75. 10.1084/jem.20151948 [PubMed: 27091843]
9. Heneka MT, Kummer MP, Stutz A, et al. (2013) NLRP3 is activated in Alzheimer's disease and contributes to pathology in APP/PS1 mice. Nature 493:674–8. 10.1038/nature11729.NLRP3 [PubMed: 23254930]
10. Xu L, He D, Bai Y (2016) Microglia-mediated inflammation and neurodegenerative disease. Mol Neurobiol 53:6709–6715. 10.1007/s12035-015-9593-4 [PubMed: 26659872]
11. Mackenzie IR, Hao CMD (1995) Role of microglia in senile plaque formation. Neurobiol Aging 16:797–804. [PubMed: 8532113]
12. Spangenberg E, Severson PL, Hohsfield LA, et al. (2019) Sustained microglial depletion with CSF1R inhibitor impairs parenchymal plaque development in an Alzheimer's disease model. Nat Commun 10:3758 10.1038/s41467-019-11674-z [PubMed: 31434879]
13. Asai H, Ikezu S, Tsunoda S, et al. (2015) Depletion of microglia and inhibition of exosome synthesis halt tau propagation. Nat Neurosci. 10.1038/nn.4132
14. Spangenberg EE, Lee RJ, Najafi AR, et al. (2016) Eliminating microglia in Alzheimer's mice prevents neuronal loss without modulating amyloid-b pathology. Brain 139:1265–81. 10.1093/brain/aww016 [PubMed: 26921617]
15. Bie B, Wu J, Foss JF, Naguib M (2019) Activation of mGluR1 mediates C1q-dependent microglial phagocytosis of glutamatergic synapses in Alzheimer's rodent models. Mol Neurobiol 56:5568–5585. 10.1007/s12035-019-1467-8 [PubMed: 30652266]
16. Dagher NN, Najafi AR, Kayala KMN, et al. (2015) Colony-stimulating factor 1 receptor inhibition prevents microglial plaque association and improves cognition in 3xTg-AD mice. J Neuroinflammation 12:139 10.1186/s12974-015-0366-9 [PubMed: 26232154]
17. Konishi H, Kiyama H (2018) Microglial TREM2/DAP12 Signaling: A Double-Edged Sword in Neural Diseases. Front Cell Neurosci 12:1–14. 10.3389/fncel.2018.00206 [PubMed: 29386999]
18. Lee S-H, Suk K (2018) Kinase-based taming of brain microglia toward disease-modifying therapy. Front Cell Neurosci 12:1–12. 10.3389/fncel.2018.00474 [PubMed: 29386999]
19. Guiet R, Poincloux R, Castandet J, et al. (2008) Hematopoietic cell kinase (Hck) isoforms and phagocyte duties - From signaling and actin reorganization to migration and phagocytosis. Eur J Cell Biol 87:527–542. 10.1016/j.ejcb.2008.03.008 [PubMed: 18538446]

20. Lowell CA, Soriano P, Varmus HE (1994) Functional overlap in the src gene family: Inactivation of hck and fgr impairs natural immunity. Genes Dev 8:387–398. 10.1101/gad.8.4.387 [PubMed: 8125254]
21. Zhang B, Gaiteri C, Bodea L-G, et al. (2013) Integrated systems approach identifies genetic nodes and networks in late-onset Alzheimer's disease. Cell 153:707–20. 10.1016/j.cell.2013.03.030 [PubMed: 23622250]
22. Ayata P, Badimon A, Strasburger HJ, et al. (2018) Epigenetic regulation of brain region-specific microglia clearance activity. Nat Neurosci 21:1049–1060. 10.1038/s41593-018-0192-3 [PubMed: 30038282]
23. Choucair N, Laporte V, Levy R, et al. (2006) Phagocytic functions of microglial cells in the central nervous system and their importance in two neurodegenerative diseases: Multiple sclerosis and Alzheimer's disease. Cent Eur J Biol 1:463–493. 10.2478/s11535-006-0038-y
24. Krady JK, Basu A, Levison SW, Milner RJ (2002) Differential expression of protein tyrosine kinase genes during microglial activation. Glia 40:11–24. 10.1002/glia.10101 [PubMed: 12237840]
25. Castillo E, Leon J, Mazzei G, et al. (2017) Comparative profiling of cortical gene expression in Alzheimer's disease patients and mouse models demonstrates a link between amyloidosis and neuroinflammation. Sci Rep 7:1–16. 10.1038/s41598-017-17999-3 [PubMed: 28127051]
26. Bonham LW, Sirkis DW, Yokoyama JS (2019) The transcriptional landscape of microglial genes in aging and neurodegenerative disease. Front Immunol 10:1–17. 10.3389/fimmu.2019.01170 [PubMed: 30723466]
27. Hsiao K, Chapman P, Nilsen S, et al. (1996) Correlative memory deficits, Abeta elevation, and amyloid plaques in transgenic mice. Science (80-) 274:99–102. 10.1126/science.274.5284.99
28. Rodriguez-Ortiz CJ, Hoshino H, Cheng D, et al. (2013) Neuronal-specific overexpression of a mutant valosin-containing protein associated with IBMPFD promotes aberrant ubiquitin and TDP-43 accumulation and cognitive dysfunction in transgenic mice. Am J Pathol 183:504–15. 10.1016/j.ajpath.2013.04.014 [PubMed: 23747512]
29. Zumkehr J, Rodriguez-Ortiz CJ, Cheng D, et al. (2015) Ceftriaxone ameliorates tau pathology and cognitive decline via restoration of glial glutamate transporter in a mouse model of Alzheimer's disease. Neurobiol Aging 36:2260–2271. 10.1016/j.neurobiolaging.2015.04.005 [PubMed: 25964214]
30. Kitazawa M, Cheng D, Tsukamoto MR, et al. (2011) Blocking IL-1 signaling rescues cognition, attenuates tau pathology, and restores neuronal β-catenin pathway function in an Alzheimer's disease model. J Immunol 187:6539–49. 10.4049/jimmunol.1100620 [PubMed: 22095718]
31. Ulrich JD, Finn MB, Wang Y, et al. (2014) Altered microglial response to Abeta plaques in APPPS1–21 mice heterozygous for TREM2. Mol Neurodegener 9:20 10.1186/1750-1326-9-20 [PubMed: 24893973]
32. Marsh SE, Abud EM, Lakatos A, et al. (2016) The adaptive immune system restrains Alzheimer's disease pathogenesis by modulating microglial function. Proc Natl Acad Sci 113:E1316–25. 10.1073/pnas.1525466113 [PubMed: 26884167]
33. Terry RD, Masliah E, Salmon DP, et al. (1991) Physical basis of cognitive alterations in Alzheimer's disease: synapse loss is the major correlate of cognitive impairment. Ann Neurol 30:572–580. 10.1002/ana.410300410 [PubMed: 1789684]
34. DeKosky ST, Scheff SW (1990) Synapse loss in frontal cortex biopsies in Alzheimer's disease: correlation with cognitive severity. Ann Neurol 27:457–464. 10.1002/ana.410270502 [PubMed: 2360787]
35. Braak H, Braak E, Bohl J (1993) Staging of Alzheimer-related cortical destruction. Eur Neurol 33:403–408. 10.1159/000116984 [PubMed: 8307060]
36. Lanz TA, Carter DB, Merchant KM (2003) Dendritic spine loss in the hippocampus of young PDAPP and Tg2576 mice and its prevention by the ApoE2 genotype. Neurobiol Dis 13:246–253. 10.1016/S0969-9961(03)00079-2 [PubMed: 12901839]
37. Cole SL, Vassar R (2007) The Alzheimer's disease Beta-secretase enzyme, BACE1. Mol Neurodegener 2:22 10.1186/1750-1326-2-22 [PubMed: 18005427]

38. Itagaki S, McGeer PL, Akiyama H, et al. (1989) Relationship of microglia and astrocytes to amyloid deposits of Alzheimer disease. J Neuroimmunol 24:173–182. [PubMed: 2808689]
39. Wegiel J, Wisniewski H (1990) The complex of microglial cells and amyloid star in three-dimensional reconstruction. Ann Neurol 81:116–24. 10.1007/bf00334499
40. Medeiros R, Kitazawa M, Passos GF, et al. (2013) Aspirin-triggered lipoxin A4 stimulates alternative activation of microglia and reduces Alzheimer disease-like pathology in mice. Am J Pathol 182:1780–1789. 10.1016/j.ajpath.2013.01.051 [PubMed: 23506847]
41. Sasaki A, Shoji M, Harigaya Y, et al. (2002) Amyloid cored plaques in Tg2576 transgenic mice are characterized by giant plaques, slightly activated microglia, and the lack of paired helical filament-typed, dystrophic neurites. Virchows Arch 441:358–367. 10.1007/s00428-002-0643-8 [PubMed: 12404061]
42. Condello C, Yuan P, Schain A, Grutzendler J (2015) Microglia constitute a barrier that prevents neurotoxic protofibrillar Aβ42 hotspots around plaques. Nat Commun 6:6176 10.1038/ncomms7176 [PubMed: 25630253]
43. Yuan P, Condello C, Keene CD, et al. (2016) TREM2 haplodeficiency in mice and humans impairs the microglia barrier function leading to decreased amyloid compaction and severe axonal dystrophy. Neuron 90:724–739. 10.1016/j.neuron.2016.05.003 [PubMed: 27196974]
44. Jansen IE, Savage JE, Watanabe K, et al. (2019) Genome-wide meta-analysis identifies new loci and functional pathways influencing Alzheimer's disease risk. Nat Genet 51:404–413. 10.1038/s41588-018-0311-9 [PubMed: 30617256]
45. Malm TM, Jay TR, Landreth GE (2015) The evolving biology of microglia in Alzheimer's disease. Neurotherapeutics 12:81–93. 10.1007/s13311-014-0316-8 [PubMed: 25404051]
46. Mosher KI, Wyss-Coray T (2014) Microglial dysfunction in brain aging and Alzheimer's disease. Biochem Pharmacol 88:594–604. 10.1016/j.bcp.2014.01.008 [PubMed: 24445162]
47. Wood JG, Zinsmeister P (1991) Tyrosine phosphorylation systems in Alzheimer's disease pathology. Neurosci Lett 121:12–16. 10.1016/0304-3940(91)90637-9 [PubMed: 1708471]
48. Dhawan G, Floden AM, Combs CK (2012) Amyloid-β oligomers stimulate microglia through a tyrosine kinase dependent mechanism. Neurobiol Aging 33:2247–2261. 10.1016/j.neurobiolaging.2011.10.027.Amyloid- [PubMed: 22133278]
49. Dhawan G, Combs CK (2012) Inhibition of Src kinase activity attenuates amyloid associated microgliosis in a murine model of Alzheimer's disease. J Neuroinflammation 9:117 10.1186/1742-2094-9-117 [PubMed: 22673542]
50. Schweig JE, Yao H, Beaulieu-Abdelahad D, et al. (2017) Alzheimer's disease pathological lesions activate the spleen tyrosine kinase. Acta Neuropathol Commun 5:69 10.1186/s40478-017-0472-2 [PubMed: 28877763]
51. Satoh J-I, Tabunoki H, Ishida T, et al. (2012) Phosphorylated Syk expression is enhanced in Nasu-Hakola disease brains. Neuropathology 32:149–57. 10.1111/j.1440-1789.2011.01256.x [PubMed: 21981270]
52. Combs CK, Karlo JC, Kao SC, Landreth GE (2001) beta-Amyloid stimulation of microglia and monocytes results in TNFalpha-dependent expression of inducible nitric oxide synthase and neuronal apoptosis. J Neurosci 21:1179–88. [PubMed: 11160388]
53. Sondag CM, Dhawan G, Combs CK (2009) Beta amyloid oligomers and fibrils stimulate differential activation of primary microglia. J Neuroinflammation 6:1 10.1186/1742-2094-6-1 [PubMed: 19123954]
54. Fan Z, Brooks DJ, Okello A, Edison P (2017) An early and late peak in microglial activation in Alzheimer's disease trajectory. Brain 40:792–803. 10.1093/brain/aww349
55. Jiang T, Wan Y, Zhang YD, et al. (2017) TREM2 overexpression has no improvement on neuropathology and cognitive impairment in aging APPswe/PS1dE9 mice. Mol Neurobiol 54:855–865. 10.1007/s12035-016-9704-x [PubMed: 26780455]
56. Mucke L, Masliah E, Yu G-Q, et al. (2000) High-level neuronal expression of Aβ1–42 in wild-type human amyloid protein precursor transgenic mice: synaptotoxicity without plaque formation. J Neurosci 20:4050–4058. [PubMed: 10818140]

57. King DL, Arendash GW (2002) Behavioral characterization of the Tg2576 transgenic model of Alzheimer's disease through 19 months. Physiol Behav 75:627–642. 10.1016/S0031-9384(02)00639-X [PubMed: 12020728]

58. Kobayashi DT, Chen KS (2005) Behavioral phenotypes of amyloid-based genetically modified mouse models of Alzheimer's disease. Genes, Brain Behav 4:173–196. 10.1111/j.1601-183X.2005.00124.x [PubMed: 15810905]

59. Taglialatela G, Hogan D, Zhang W-R, Dineley KT (2009) Intermediate- and long-term recognition memory deficits in Tg2576 mice are reversed with acute calcineurin inhibition. Behav Brain Res 200:95–9. 10.1016/j.bbr.2008.12.034 [PubMed: 19162087]

60. Farr SA, Erickson MA, Niehoff ML, Banks WA MJ (2014) Central and peripheral administration of antisense oligonucleotide targeting amyloid-β protein precursor improves learning and memory and reduces neuroinflammatory cytokines in Tg2576 (AβPPswe) mice. J Alzheimer's Dis 40:1005–1016. 10.3233/JAD-131883.Central [PubMed: 24577464]

61. Guillot-Sestier MV, Doty KR, Gate D, Rodriguez J Jr, Leung BP, Rezai-Zadeh KTT (2015) Il10 Deficiency Rebalances Innate Immunity to Mitigate Alzheimer-Like Pathology. Neuron 85:534–548. 10.1016/j.neuron.2014.12.068 [PubMed: 25619654]

62. Jay TR, Hirsch XAM, Broihier XML, et al. (2017) Disease Progression-Dependent Effects of TREM2 Deficiency in a Mouse Model of Alzheimer's Disease. J Neurosci 37:637–647. 10.1523/JNEUROSCI.2110-16.2017 [PubMed: 28100745]

63. Nizami S, Di Daniel E, Roberts HH, Cowley SA (2019) Microglial inflammation and phagocytosis in Alzheimer's disease: Potential therapeutic targets. Br J Pharmacol 176:3515–3532. 10.1111/bph.14618 [PubMed: 30740661]

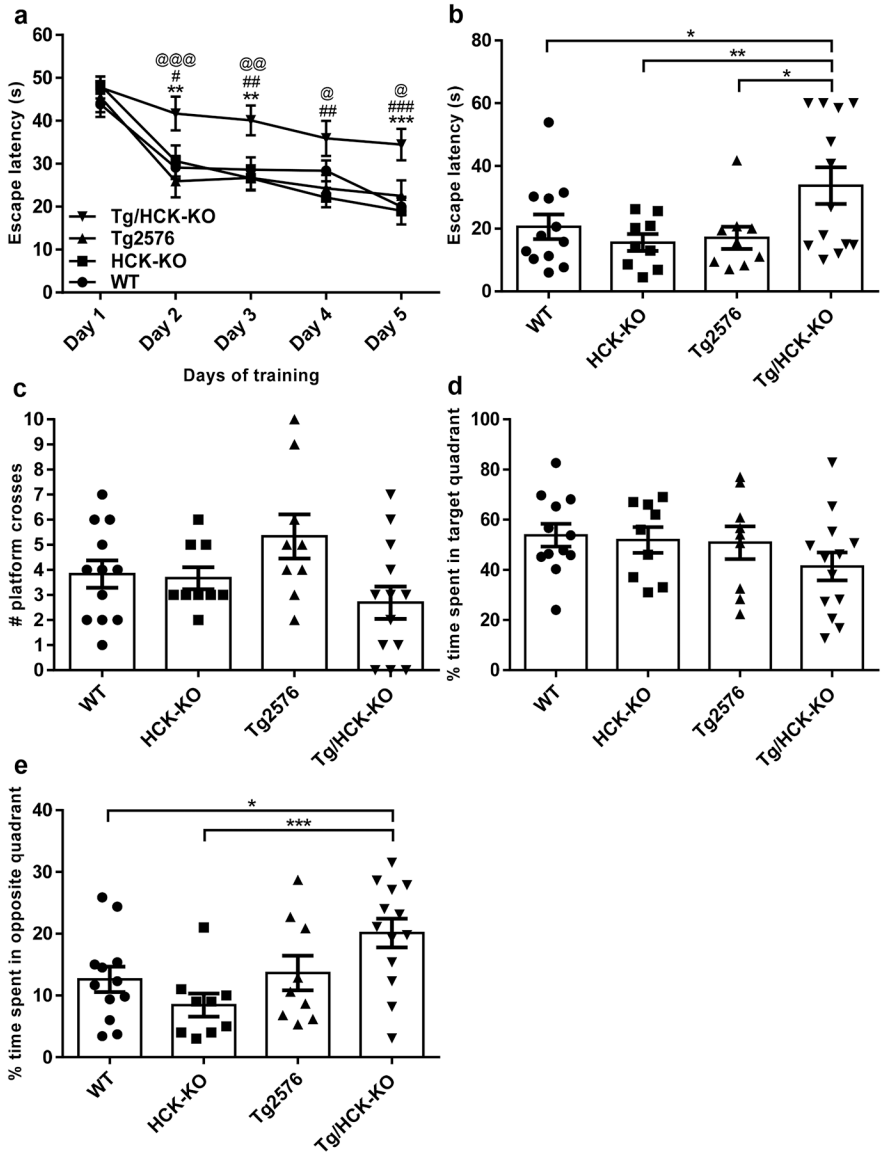

Fig. 1.

Genetic ablation of HCK significantly impaired hippocampal-dependent spatial memory in Tg2576 mice as evident in MWM task. (**a-e**) WT, HCK-KO, Tg2576 and Tg/HCK-KO mice of 10–12 months were trained for five days, and Tg/HCK-KO mice took significantly longer escape latency than WT, HCK-KO or Tg2576 mice from the second to the fifth day of training (**a**). Data are expressed as mean ± SEM with n = 9–15, ** $p < 0.01$ and *** $p < 0.001$ relative to WT mice; $^{\#}$ $p < 0.05$, $^{\#\#}$ $p < 0.01$ and $^{\#\#\#}$ $p < 0.001$ relative to HCK-KO mice; $^{@}$ $p < 0.05$, $^{@@}$ $p < 0.01$ and $^{@@@}$ $p < 0.001$ relative to Tg2576 mice (Repeated measures two-way ANOVA with multiple comparisons of performance by genotype per day). At the 1 wk test after the last MWM training, Tg/HCK-KO mice again took significantly longer escape latency than WT, HCK-KO or Tg2576 mice in finding the platform (**b**). Tg/HCK-KO mice also exhibited the lowest, but not significant, number of platform crosses (**c**) and % time spent in target quadrant (**d**), but the highest % time spent in

the opposite quadrant (**e**) than the other genotypes. However, they were not significantly different from that of Tg2576 mice. Data are expressed as mean ± SEM with n = 9–13, * $p < 0.05$, ** $p < 0.01$ and *** $p < 0.001$ between indicated genotypes

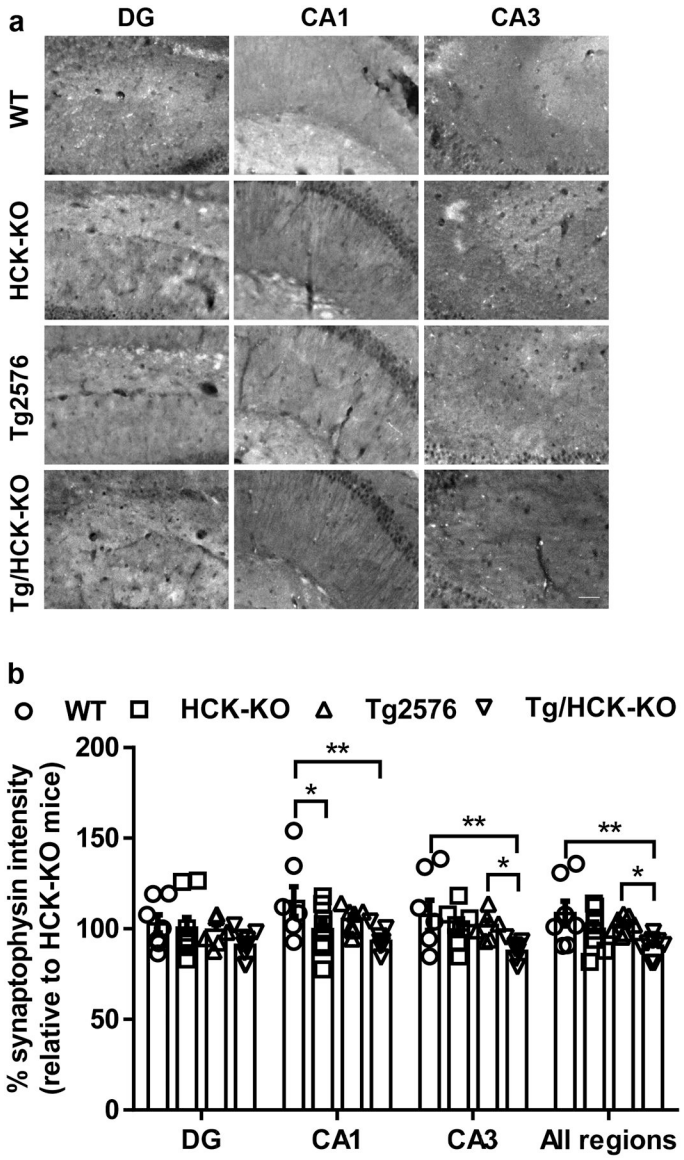

Fig. 2.

HCK deficiency in Tg2576 mice substantially reduced intensity of synaptophysin in the hippocampal CA1, CA3 and overall regions. (**a)** Representative images of synaptophysin (pre-synaptic protein marker) at the DG, CA1 and CA3 regions of the hippocampus of WT, HCK-KO, Tg2576 and Tg/HCK-KO mice (11–13 months old). Scale bar, 50 μm. (**b**) Quantitative analyses of % synaptophysin intensities in WT, HCK-KO, Tg2576 and Tg/HCK-KO mice taken relative to that of HCK-KO mice revealed significant reduction in Tg/HCK-KO mice at the CA1 (compared to WT mice), CA3 (compared to WT and Tg2576 mice) and all three regions (compared to WT and Tg2576 mice). Data are expressed as mean ± SEM from three sections per mouse with n = 7–9. * $p < 0.05$ and ** $p < 0.01$ between indicated genotypes

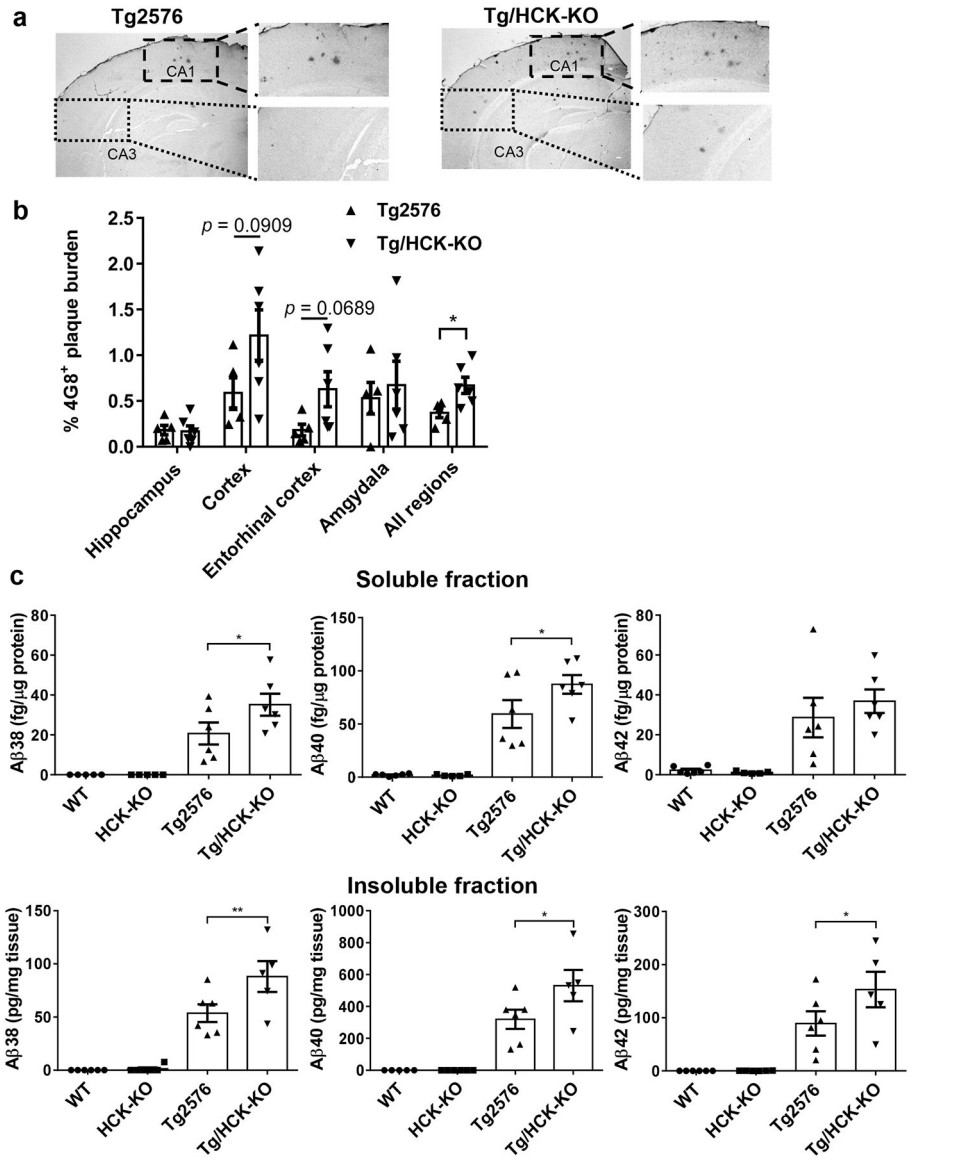

Fig. 3.

Eliminating HCK in Tg2576 mice drastically increased Aβ plaque burden and brain Aβ level. (**a**) Representative images of 4G8-positive Aβ plaques found in the cortical and hippocampal regions of 11–13 months old Tg2576 and Tg/HCK-KO mice. Cortical regions near CA1 and CA3 were being quantified as shown in the dotted marking boxes. Scale bar, 100 μm. (**b**) Quantitative analysis of 4G8-positive Aβ plaques area found in the hippocampus, cortex, entorhinal cortex, amygdala or combined regions of Tg2576 (n = 5) and Tg/HCK-KO (n = 6) mice. Significant accumulation of 4G8-positive plaques were observed in the combined regions of Tg/HCK-KO mice. Data are expressed as mean ± SEM from five sections per mouse. * $p < 0.05$ relative to Tg2576 mice. (**c**) MSD quantification of detergent-soluble (top) and -insoluble (bottom) Aβ38 (left), Aβ40 (middle) and Aβ42 (right) in protein lysates of mouse hippocampus. Lysates from WT, HCK-KO, Tg2576 and Tg/HCK-KO mice were analyzed at n = 5–6. Substantial augmentation of soluble Aβ38 and

Aβ40 and insoluble Aβ38, Aβ40 and Aβ42 were detected in Tg/HCK-KO mice when compared to Tg2576 mice. * $p < 0.05$ and ** $p < 0.01$ between indicated genotypes

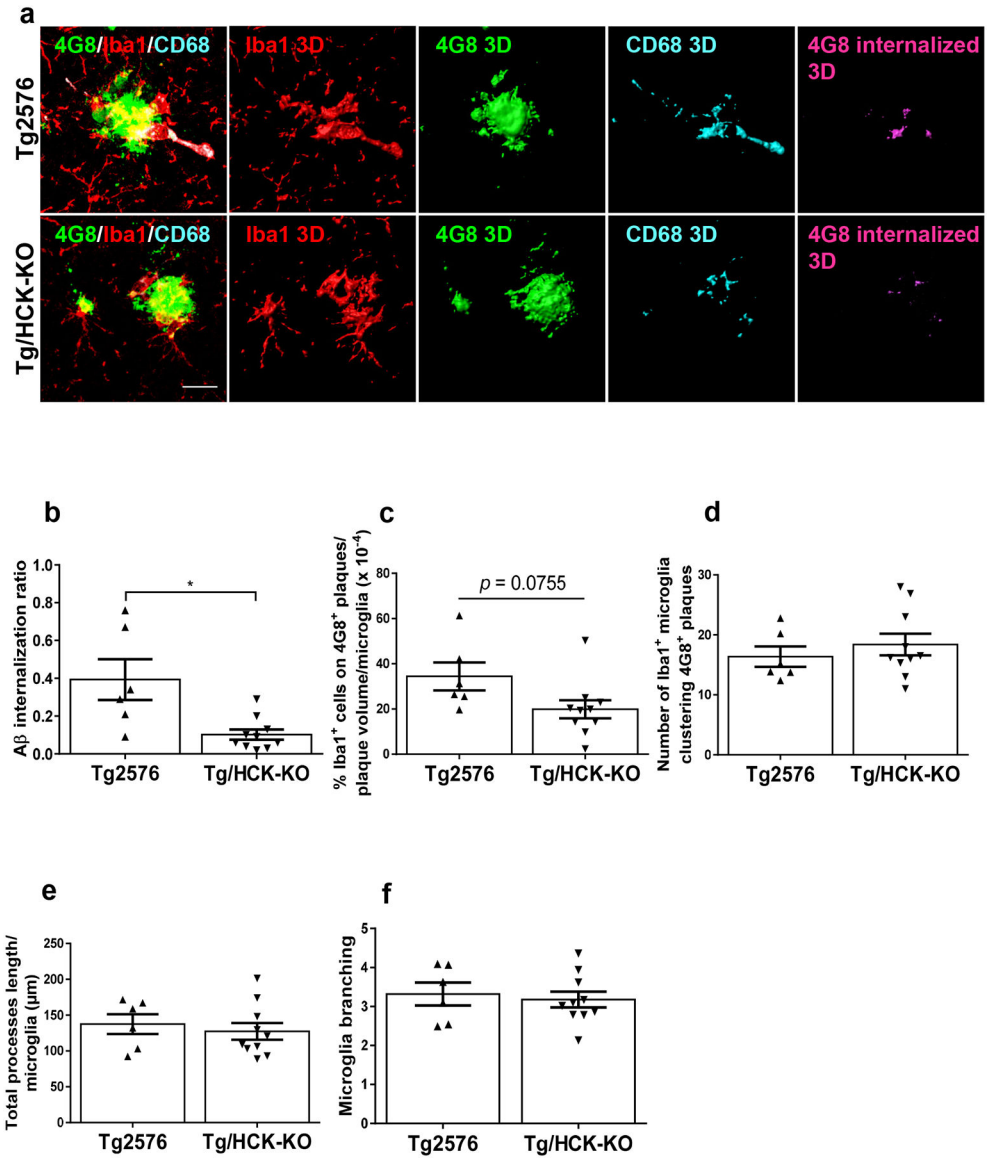

Fig. 4.

Knocking out HCK in Tg2576 mice significantly attenuated Aβ internalization in microglia and reduced microglia coverage on 4G8-positive plaques. (**a**) Representative images of 4G8-positive plaques (green) clustered by Iba1-positive microglia (red) and CD68-positive phagolysosomes (cyan) in Tg2576 (top) and Tg/HCK-KO (bottom) mice (11–13 months old). Three dimensional (3D) reconstruction of respective signals as well as that of 4G8-positive plaques internalized in CD68- and Iba1-positive microglial phagolysosomes were shown. Scale bar, 20 μm. (**b**) Quantitative analysis of Aβ internalization ratio revealed a 74% reduction in microglial phagocytic activity in Tg/HCK-KO mice. Aβ internalization ratio was calculated by normalizing volume of Aβ accumulated within microglial phagolysosomes to microglia number on the plaque(s) and Aβ plaque volume within the region. (**c**) Quantitative analysis of % Iba1-positive cells clustering 4G8-positive plaques per plaque volume per cell (microglial coverage) revealed near significant reduction in Tg/HCK-

KO mice. On the other hand, volumetric and Imaris automated analyses of Iba1-positive microglia clustering around 4G8-positive plaques did not show apparent differences in the number of microglia (**d**), total processes length per microglia (**e**), nor microglia branching (**f**) between the genotypes. Plaques of diameter ≥ 30 μm were analyzed in the hemibrains (excluding the thalamus) of 6 Tg2576 (n = 54) and 10 Tg/HCK-KO (n = 45) mice. Data are expressed as mean ± SEM from one section per mouse. * $p < 0.05$ relative to Tg2576 mice

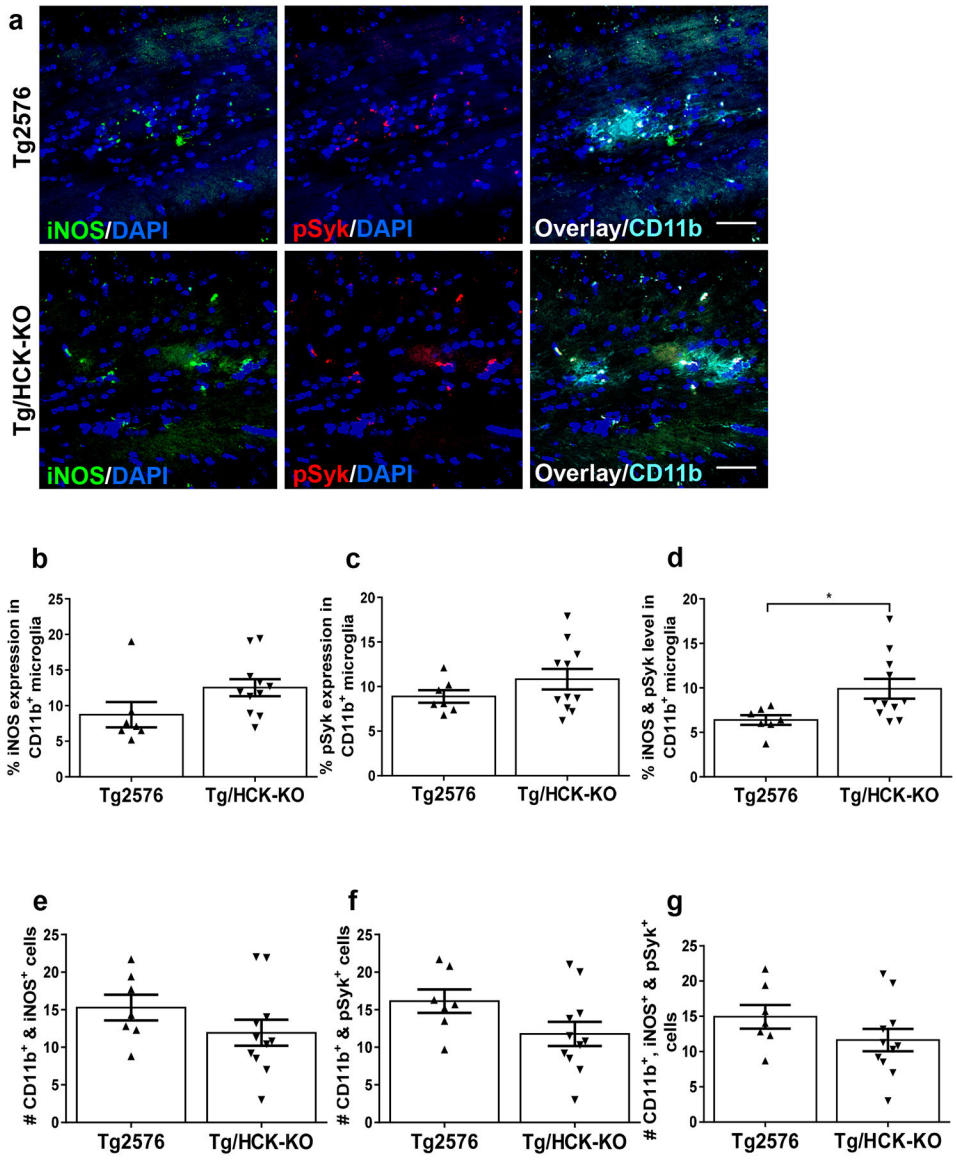

Fig. 5.

Depleting HCK in Tg2576 mice significantly elevated iNOS and pSYK expression in CD11b$^+$ microglial clusters. (**a**) Representative images of iNOS (green) and pSYK (red) expressing in CD11b$^+$ (cyan) microglial clusters in Tg2576 (top) and Tg/HCK-KO (bottom) mice (11–13 months old). Nuclei stained with DAPI were shown in blue. Scale bar, 20 μm. (**b-d**) Quantitative analyses of either % iNOS (**b**), pSYK (**c**), or both iNOS and pSYK (**d**) in the CD11b$^+$ microglial clusters showed higher expression in HCK-depleted Tg2576 mice, but was only significant in the last analysis. (**e-g**) Clusters of microglial cells positively stained for CD11b and iNOS (**e**), CD11b and pSYK (**f**), as well as CD11b, iNOS and pSYK (**g**) were also counted, and were not significantly different between genotypes. Microglial clusters were analyzed in the hemibrains (excluding the thalamus) of 7 Tg2576 (n = 34) and 11 Tg/HCK-KO mice (n = 67). Data are expressed as mean ± SEM from one section per mouse. * $p < 0.05$ relative to Tg2576 mice

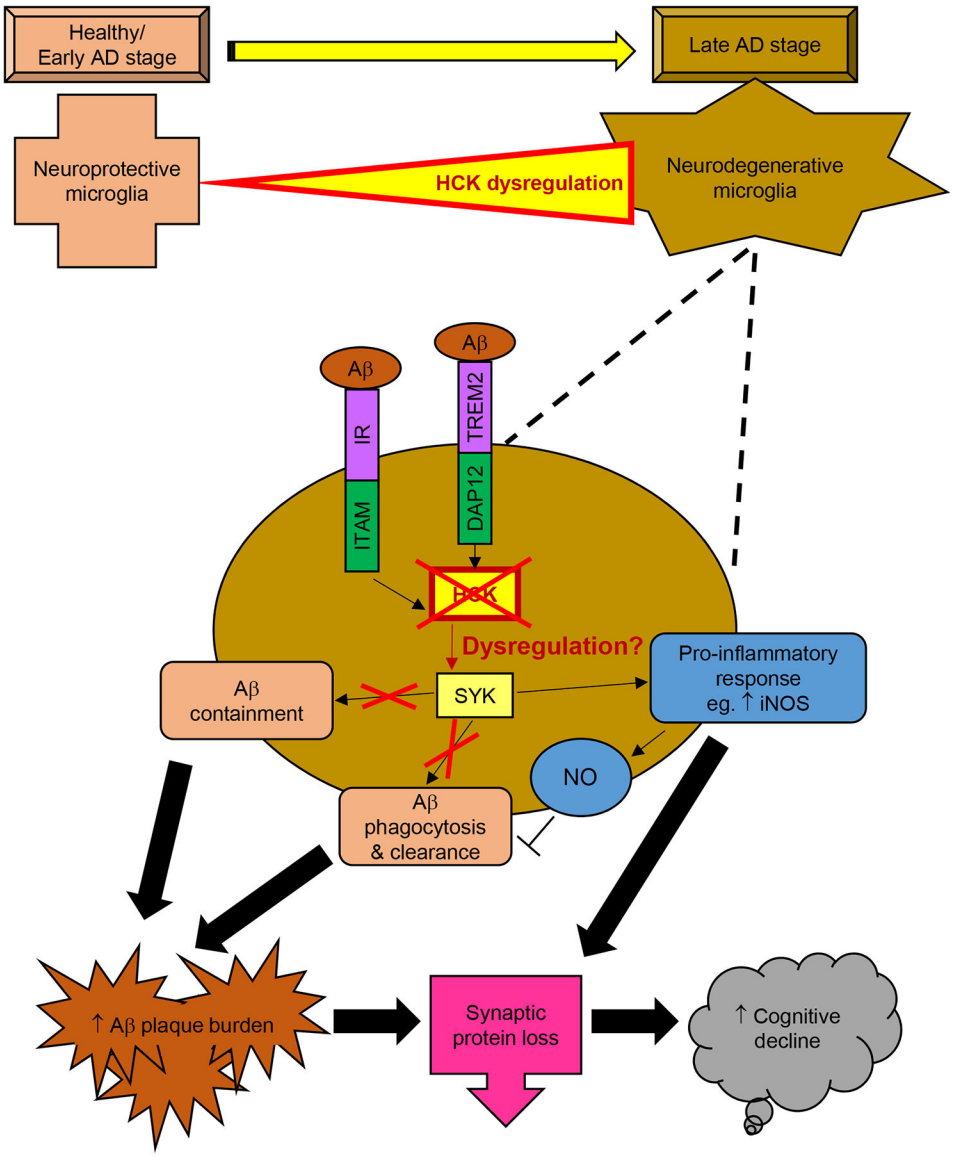

Fig. 6.

Schematic diagram proposing detrimental effects of microglial HCK dysregulation in AD progression. Based on the exacerbated neuropathology observed upon HCK deletion in two mouse models of AD, we speculate that HCK dysregulation switched microglia from neuroprotective phenotype to neurodegenerative as observed in late stage AD. In the absence of regulated HCK, which is the key regulator of phagocytic activity among the SFKs, Aβ-stimulated microglial phagocytosis through IR such as TREM2, its corresponding immunoreceptor tyrosine-based activation motif (ITAM) - DAP12, and downstream kinase - SYK will be impaired, leading to attenuated Aβ clearance and accumulated Aβ plaques in the brain. Microglial containment of Aβ dense core plaques will also be compromised, contributing to more aberrant plaque build-up. Pro-inflammatory response, such as increase levels of iNOS, will be triggered, releasing nitric oxide (NO) that further inhibits microglial

phagocytosis. The accumulated plaques burden and elevated pro-inflammatory cytokine levels in the brain eventually lead to synaptic protein loss that resulted in cognitive decline.